Transition from Exponentially Damped to Finite-Time Arrest Liquid Oscillations Induced by Contact Line Hysteresis

Benjamin Dollet, Elise Lorenceau, François Gallaire

Transition from Exponentially Damped to Finite-Time Arrest Liquid Oscillations Induced by Contact Line Hysteresis

Benjamin Dollet,[1] Élise Lorenceau,[1] and François Gallaire[2]
[1]Université Grenoble Alpes, CNRS, LIPhy, 38000 Grenoble, France
[2]Laboratory of Fluid Mechanics and Instabilities, École Polytechnique Fédérale de Lausanne, 1015 Lausanne, Switzerland

(Received 18 July 2019; revised manuscript received 21 November 2019; accepted 5 February 2020; published 13 March 2020)

To clarify the role of wetting properties on the damping of liquid oscillations, we studied the decay of oscillations of liquid columns in a U-shaped tube with controlled surface conditions. In the presence of sliding triple lines, oscillations are strongly and nonlinearly damped, with a finite-time arrest and a dependence on initial amplitude. We reveal that contact angle hysteresis explains and quantifies this solidlike friction.

DOI: 10.1103/PhysRevLett.124.104502

Sloshing, i.e., the oscillations of liquids in tanks, is an issue in mechanical engineering and daily life. It constitutes a risk against the stability of tankers [1] and spacecraft, and may lead to liquid spilling [2]. It is therefore important to understand its damping. Sloshing is classically modeled by determining the oscillation modes compatible with a given tank shape using potential flow theory, supplemented by viscous dissipation coming from bulk potential flow and Stokes boundary layers along walls [1,3]. However, lab-scale studies have revealed that dissipation predicted as such underestimates the experiments, which also indicates a dependence on the wall material [4,5]. This has been tentatively ascribed to a source of dissipation localized in the vicinity of the air-liquid-solid triple line. It echoes several other configurations where wetting conditions affect macroscopic flows, like Faraday waves [6], drop fall down inclines [7,8], Torricelli's law [9], or capillary rise [10,11]. However, there is no quantitative prediction relating wetting properties to sloshing damping. In this Letter, we solve this long-standing problem in the simplest sloshing configuration: a liquid column oscillating in a U-shaped tube, which may be described by a single degree of freedom, in contrast with the infinite number of modes describing sloshing in tanks [1,3].

We used two U-shaped glass tubes (Dutscher). One was rendered hydrophilic using plasma treatment, and the other hydrophobic by silanization with a silicon reagent (Sigmacote, Sigma-Aldrich). The two straight arms of the tubes have a constant inner radius $a = 8.15 \pm 0.15$ mm [Fig. 1(a)], the curved part having a significantly smaller cross section [not drawn in Fig. 1(a) for simplicity]. The tubes were carefully rinsed and dried with nitrogen between each run, ensuring reproducible wetting conditions. We used two liquids: ultrapure water (MilliQ) and absolute ethanol (VWR). We characterized their wetting properties by depositing droplets on glass slides treated similarly and simultaneously as the tubes, and slowly injecting or withdrawing liquid from these droplets. From the onset of contact line motion, we measured values for the advancing (θ_a) and receding (θ_r) contact angles. Ethanol wetted perfectly the hydrophilic slide; for water, $\theta_a = (15 \pm 5)°$ and no significant receding contact angle could be measured. On the hydrophobic slide, $\theta_r = (68 \pm 10)°$ and $\theta_a = (93 \pm 2)°$ for water, and for ethanol, $\theta_r = (28 \pm 2)°$ and $\theta_a = (34 \pm 2)°$.

We studied the free decay of liquid oscillations as follows. We injected a controlled volume in the tube, making a liquid column of length ℓ' (controlled within 1 mm) along the tube centerline [Fig. 1(a)]. We plugged one arm with a thin membrane under tension. We injected through a flexible tube a controlled volume of air in the resulting trapped air pocket, creating an initial height imbalance $2h_0$ between the two contact lines. We pierced the membrane with a needle, ensuring controlled initial conditions, and recorded the subsequent oscillations of one of the two interfaces with a camera (Thorlabs). By image analysis, we extracted from the movies the position

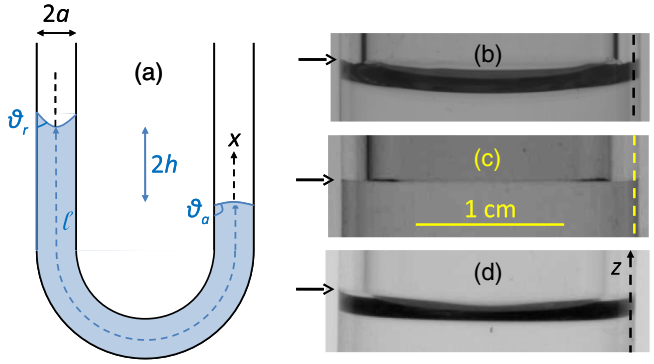

FIG. 1. (a) Sketch of the experiment. Snapshots of the air-liquid interface for (b) water in the hydrophilic tube, and (c) water and (d) ethanol in the hydrophobic tube. Arrows indicate the location of the contact line, which position is measured along the dashed lines.

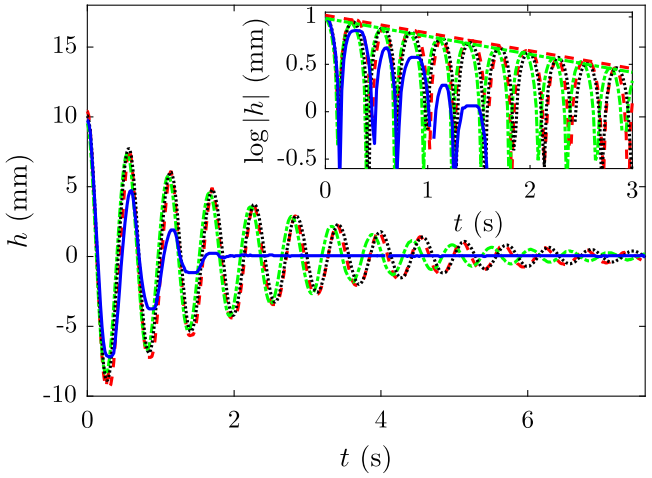

FIG. 2. Plot of the interface height h vs time t, for water in the hydrophobic (blue plain curve) and hydrophilic (green dash-dotted curve) tubes, and ethanol in the hydrophobic (red dashed curve) and hydrophilic (black dotted curve) tubes, with the same column length $\ell' = 10.6$ cm and initial amplitude $h_0 = 10.0 \pm 0.3$ mm. Inset: plot of $\log|h|$ vs t. The straight lines are the best fits of exponentially decaying envelopes.

$h(t)$ of the contact line along one given vertical line [Figs. 1(b)–1(d)]; $h = 0$ corresponds to equilibrium. We checked that the contact line remains horizontal at all times.

Figure 2 shows the oscillation decay for both liquids in both tubes, for the same column length and initial amplitude. For water, the effect of wetting conditions is striking: the oscillations are much more damped in the hydrophobic tube. Moreover, the damping dynamics differs: while the oscillations are exponentially damped in the hydrophilic tube, the time evolution of $\log|h|$ displays a concave envelope for the hydrophobic tube (inset of Fig. 2) with a finite-time arrest of the oscillations, in marked contrast with the classical view of oscillations damped by viscous effects scaling linearly with velocity. Such increasing damping rate as the amplitude of motion diminishes is known to lead to finite-time arrest in different systems [12,13]. To investigate further this qualitative difference in damping, we study the decay of water oscillations for different initial amplitudes h_0. For the hydrophilic tube, the time evolution of h/h_0 is independent of h_0, and is well captured by an exponential decay [Fig. 3(a)]. On the contrary, for the hydrophobic tube, the time evolution of h/h_0 depends on h_0: the smaller the initial amplitude, the faster the decay [Fig. 3(b)] and the shorter the time of arrest of oscillations [inset of Fig. 3(b)]. Figures 2 and 3 thus suggest that damping is linear, respectively, nonlinear, for the hydrophilic, respectively, hydrophobic, tube. For ethanol, the oscillations are exponentially damped [Fig. 3(c)], without dependence on the tube (Fig. 2), unlike water. Henceforth, for simplicity, the measurements reported for ethanol are for the hydrophobic tube only.

Visual inspection reveals another difference between water in the hydrophobic tube and the other cases, where at its first descent, the moving meniscus deposits a thin film along the wall, and during most of the subsequent oscillations, the interface slides over this film [see, e.g., inset of Fig. 3(c)]. The conditions under which a liquid in partial wetting can deposit a film in our experiments are discussed in the Supplemental Material [14], and agree with existing predictions [18]. Rigorously speaking, what we track is thus an apparent contact line between the liquid bulk and the film. On the contrary, for water in the hydrophobic tube, no film seems to be deposited, hence the water column is bounded by oscillating sliding triple lines.

Since bulk dissipation is always present, the qualitative difference in damping comes from the different wetting conditions. If a film is present, some dissipation comes from the dynamic menisci between the film and the bulk of liquid. Such a dissipation scales nonlinearly with the

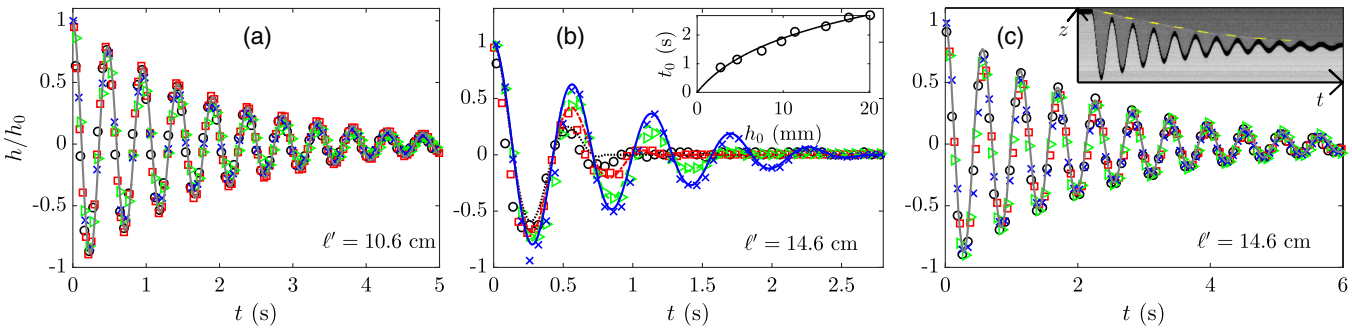

FIG. 3. Plot of the interface height h rescaled by the initial amplitude h_0 vs time t for water in the (a) hydrophilic and (b) hydrophobic tube, and (c) for ethanol. Values of ℓ' are indicated on each graph, and $h_0 = 2.7 \pm 0.1$ (circle), 5.2 ± 0.5 (square), 10.3 ± 0.5 (slanted triangle), and 20.3 ± 0.5 mm (cross mark). In (a) and (c), the plain curves are fit $h = h_0 e^{-\alpha\omega_0 t/2}\cos\omega_0 t$, with best fitting parameters: (a) $\omega_0 = 13.2$ rad/s and $\alpha = 0.076$, and (c) $\omega_0 = 11.1$ rad/s and $\alpha = 0.083$. (b) Data are fitted by Eq. (3) with $\alpha = 0.12$ as free fitting parameter common for all experiments and μ given by Eq. (2) for $h_0 = 2.7$ (dotted curve), 5.2 (dash-dotted curve), 10.3 (dashed curve), and 20.3 mm (plain curve). Insets: (b) Plot of the arrest time of oscillations t_0 vs h_0. The curve comes from the model $t_0 = (2/\alpha\omega_0)\ln[1 + (\pi/4)(\alpha/\mu)]$ with $\alpha = 0.12$. (c) Raw space-time diagram along the dashed line of Fig. 1(d), showing (highlighted by yellow dashes) the draining top of the thin film deposited at the first descent.

sliding velocity [19,20]. In another context, it explains the strong damping of sloshing by foam, where many dynamic menisci are present all along the bubbles against the walls [13,21]. However, the fact that the oscillations show an exponential decay and no dependence on the initial amplitude suggests that, for ethanol and water in the hydrophilic tube, dissipation in dynamic menisci is negligible compared to bulk dissipation, as checked in the Supplemental Material [14]. For water in the hydrophobic tube, some dissipation comes from the imbalance between the advancing and the receding contact angles which simultaneously, and alternatively, exist at both ends of the oscillating column. This angle difference provides a strongly nonlinear resistive force, already essentially present in statics; this frictionlike force is known to pin small enough water droplets on glass plates. We now model its effect on the oscillation dynamics.

We model the oscillations of an incompressible liquid column of curvilinear length ℓ in a tube of constant radius a. We aim at predicting the height $h(t)$ of one contact line (the other being at height $-h$). When $h \neq 0$, the column oscillates and relaxes towards equilibrium under the action of gravity, viscous friction, and contact line friction. To simplify, we take h as the sole degree of freedom; we thus model the motion of the contact lines, but not of the air-liquid interfaces.

In an oscillatory motion of angular frequency ω, for a liquid of kinematic viscosity ν, viscous effects act over a thickness of order $\delta = \sqrt{\nu/\omega}$ from walls [22]. In our experiments, the period is of order 0.5 s and $\nu = 10^{-6}$ m^2/s, hence $\delta \approx 0.3$ mm $\ll a$. Hence, the column experiences mostly a pluglike flow, except close to the interfaces and in a thin boundary layer close to the tube wall, and notwithstanding possible secondary flows within the curved part of the tube [23]. To estimate liquid inertia, we thus assume that the liquid has a uniform velocity $\dot{h}$, with dots denoting time derivatives. The equation of motion is then $\pi\rho a^2 \ell \ddot{h} = F_g + F_v + F_c$, with forces due to gravity (F_g), viscous friction (F_v), and contact line friction in the presence of triple lines (F_c), as for water in the hydrophobic tube; if they are absent, as for ethanol or water in the hydrophilic tube, $F_c = 0$.

Gravity force stems from the fall of the mass of liquid of height $2h$ between the two interfaces, hence $F_g = -2\pi\rho g a^2 h$.

Viscous effects depend on whether the flow is laminar or turbulent, which would lead, respectively, to $F_v \propto \dot{h}$ or $\dot{h}^2$. Contrary to the classical Reynolds criterion for steady Poiseuille flows in straight tubes, there is no clear existing criterion for the onset of turbulence in curved tubes [23]; Biery [24] established empirically that turbulence sets in for $B = h_0^2\omega/\nu$ larger than 3×10^4. For $h_0 \approx 1$ cm and $\omega \approx 10$ rad/s, we have $B \approx 10^3$ in our experiments, suggesting a laminar regime. We henceforth assume that $F_v = -\alpha' \dot{h}$. We have also checked that $F_v \propto -|\dot{h}|\dot{h}$ does not fit our measurements (data not shown).

For water in the hydrophobic tube, one of the contact lines is advancing while the other is receding. Owing to contact angle hysteresis, the water column experiences a force corresponding to the different projections of the surface tension forces at the contact lines along the direction of motion. Hence, $F_c = 2\pi a\gamma(\cos\theta_a - \cos\theta_r)\mathrm{sign}(\dot{h})$.

We introduce dimensionless height $\bar{h} = h/h_0$ and time $\bar{t} = \omega_0 t$, with $\omega_0 = \sqrt{2g/\ell}$ the eigenfrequency. The equation of motion becomes

$$\frac{d^2\bar{h}}{d\bar{t}^2} + \bar{h} = -\alpha\frac{d\bar{h}}{d\bar{t}} - \mu\,\mathrm{sign}\frac{d\bar{h}}{d\bar{t}}, \tag{1}$$

with two dimensionless dissipation parameters: a viscous coefficient $\alpha = \alpha'\omega_0/2\pi\rho g a^2$ taken as an adjustable parameter, and a friction coefficient

$$\mu = \frac{\gamma(\cos\theta_r - \cos\theta_a)}{\rho g a h_0}. \tag{2}$$

The initial conditions are $\bar{h} = 1$ and $d\bar{h}/d\bar{t} = 0$ at $\bar{t} = 0$.

Equation (1) can be solved numerically or piecewise analytically, but most insight comes from its analytical resolution by the multiple-scale method in the limit of small damping $\alpha \ll 1$ and $\mu \ll 1$, yielding the solution of Eq. (1) (see Supplemental Material [14] for the derivation):

$$\bar{h}(\bar{t}) = \left[-\frac{4}{\pi}\frac{\mu}{\alpha} + \left(\frac{4}{\pi}\frac{\mu}{\alpha} + 1\right)e^{-\alpha\bar{t}/2}\right]\cos\bar{t}, \tag{3}$$

if $\bar{t} \leq \bar{t}_0$, and $\bar{h} = 0$ if $\bar{t} \geq \bar{t}_0$, with $\bar{t}_0 = (2/\alpha)\ln[1 + (\pi/4)(\alpha/\mu)]$ the time of arrest of the oscillations. The envelope shape varies from the classical exponential damping as $\alpha \gg \mu$ (no nonlinear dissipation) to a linear decay in time as $\mu \gg \alpha$, like in solid friction.

We now compare the model to our measurements. We start with the prediction of the eigenfrequency. To do so, we measure the frequency of the damped oscillations for ethanol in the hydrophobic tube, for which the oscillations are mildly damped [Fig. 3(c)], hence the discrepancy between the eigenfrequency and the frequency of the damped oscillations negligible [25]. Technically, we take the Fourier transform $\tilde{h}(\omega)$ of $h(t)$, and extract the frequency as the peak of the power spectrum $|\tilde{h}(\omega)|^2$. For an accurate comparison, we must correct for the aforementioned fact that the tube section is reduced in its curved part. To do so in good approximation, we show in the Supplemental Material [14] that it suffices to define ℓ as the sum of ℓ' and of an excess length defined from the cross-section variations. In the inset of Fig. 4, we plot the oscillation period versus ℓ: it agrees with the prediction $\omega_0 = \sqrt{2g/\ell}$ within 2.6%. Since this prediction is independent on liquid properties, we assume that it also holds for water. Concerning damping, in the absence of contact line friction, Eq. (3) becomes: $h(t) = h_0 e^{-\sigma t}\cos\omega_0 t$, with $\sigma = \alpha\omega_0/2$. Figures 3(a) and 3(c) show that the data for

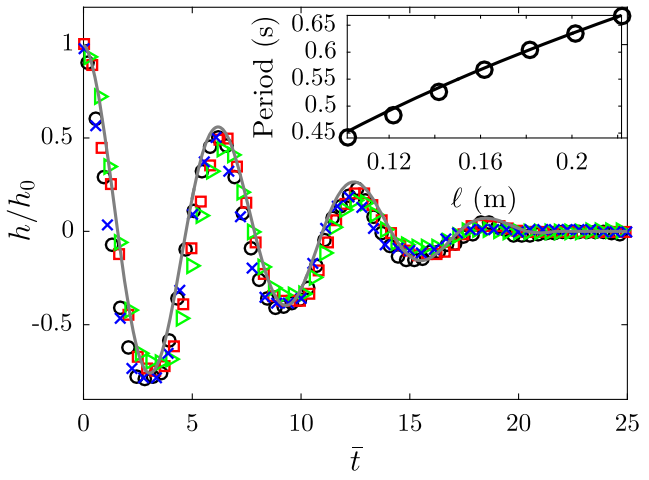

FIG. 4. Plot of the rescaled height $\bar{h} = h/h_0$ for $h_0 = 9.3 \pm 0.7$ mm as a function of the rescaled time $\bar{t} = \omega_0 t$ for water in the hydrophobic tube, for $\ell = 16.2$ (cross mark), 18.2 (slanted triangle), 20.2 (square), and 22.2 cm (circle). The curve is given by Eq. (3) with $\alpha = 0.12$ as determined from the fit in Fig. 3(b), and μ given by Eq. (2). Inset: plot of the period of the oscillations vs ℓ for ethanol in the hydrophobic tube. The curve is the prediction $T = 2\pi\sqrt{\ell/2g}$.

water in the hydrophilic tube and for ethanol agree with this prediction, with fitting parameters $\alpha_{\text{water}}^{\text{philic}} = 0.076$ and $\alpha_{\text{eth}} = 0.083$.

For water in the hydrophobic tube, we fit the data with the dimensional version of Eq. (3): $h(t) = h_0\{-(4/\pi)(\mu/\alpha) + [(4/\pi)(\mu/\alpha) + 1]e^{-\alpha\omega_0 t/2}\}\cos\omega_0 t$, with α a fitting parameter and μ predicted by Eq. (2). Although α might depend on ℓ and h_0, there is no prediction which we can rely on; hence, we simply take this parameter as a constant that we fit once and for all experiments. Figure 3(b) shows that the data are very well fitted by the model with best fitting parameter $\alpha_{\text{water}}^{\text{phobic}} = 0.12$, except for the lowest value of h_0 for which the model slightly underestimates the time of arrest of the oscillations t_0. The inset of Fig. 3(b) displays t_0 as a function of h_0, showing an excellent agreement with the model.

To further test the model, we compare its predictions with measurements for water in the hydrophobic tube at fixed h_0 but various ℓ. An important prediction of the model is that all data should then collapse on the same master curve once rescaled on the dimensionless form $\bar{h}(\bar{t})$ given by Eq. (3). Figure 4 shows that it is indeed the case in a very good approximation. This good agreement suggests that our model includes the correct dissipations.

However, surprisingly, for water, the fitted viscous coefficient for the hydrophobic tube $\alpha_{\text{water}}^{\text{phobic}} = 0.12$ is larger than for the hydrophilic tube $\alpha_{\text{water}}^{\text{philic}} = 0.076$. It is also larger than that for ethanol ($\alpha_{\text{eth}} = 0.083$), despite the larger kinematic viscosity of ethanol ($\nu_{\text{eth}} = 1.4 \times 10^{-6}$ m^{2}s, while $\nu_{\text{water}} = 1.0 \times 10^{-6}$ m^{2}s). This suggests that contact line sliding increases significantly the viscous dissipation, more precisely the damping proportional to velocity. To confirm this hypothesis and discard possible fitting artifacts, we experimentally quantified the relaxation of the air-water interface in the hydrophobic tube once the contact line is pinned; see Supplemental Material [14] for details. Briefly, this relaxation is well fitted by an exponential decay, with a damping coefficient $\sigma_{\text{water}}^{\text{pinned}}$ which depends significantly neither on ℓ nor on h_0. Averaging over all experiments yields $\sigma_{\text{water}}^{\text{pinned}} = 0.38 \pm 0.02\,\text{s}^{-1}$, hence $\sigma_{\text{eth}}/\sigma_{\text{water}}^{\text{pinned}} = 1.2 = \sqrt{\nu_{\text{eth}}/\nu_{\text{water}}}$, as expected for unsteady viscous flows [22].

Actually, viscous dissipation specifically associated with contact line sliding is known for long, and implies that the advancing, respectively, receding, contact angle increases, respectively, decreases, with the sliding velocity V. When V is constant, this is expressed by the Cox-Voinov (CV) law [7,26,27]: $\theta_a^3 = \theta_{a,0}^3 + 9A\rho\nu V/\gamma$ and $\theta_r^3 = \theta_{r,0}^3 - 9A\rho\nu V/\gamma$, where $A \simeq 15$ [28]. It is difficult to probe the instantaneous values of the contact angles inside the tube [Fig. 1(c)], but we can test their velocity dependences predicted by Cox-Voinov law; they increase the value of the parameter μ given by Eq. (2), and give rise to an extra effective viscous coefficient α_{CV}. More precisely, taking $V = |\dot{h}| \approx h_0\omega_0 \approx 0.1$ m/s in our experiments, we evaluate $9A\rho\nu V/\gamma \approx 0.2$, 1 order of magnitude smaller than $\theta_{r,0}^3 = 1.7$ and $\theta_{a,0}^3 = 4.3$; we can then linearize the Cox-Voinov law inserted in Eq. (2) to get $\mu = \mu_0 + \alpha_{\text{CV}}\dot{h}$ with $\alpha_{\text{CV}} = 3A\nu\omega_0/ga$. This extra effective viscous coefficient is evaluated as $\alpha_{\text{CV}} = 0.006$, which is too small to explain the mismatch between the viscous dissipation for water in the sliding phase and in the pinned phase. In particular, $\alpha_{\text{water}}^{\text{phobic}} - \alpha_{\text{CV}} = 0.11$ remains larger than $\alpha_{\text{water}}^{\text{philic}}$. This altogether suggests that part of the viscous (more precisely, velocity-linear) dissipation close to sliding contact lines remains elusive.

The underestimation of viscous effects by Cox-Voinov law has been pinpointed in other studies, especially on drop motion [29,30]. There has been attempts to explain the "missing" dissipation by marrying molecular effects at triple lines with hydrodynamic approaches [31,32]; however, there is no current consensus [33]. Moreover, Cox-Voinov law applies only for steady motions, and little remains known on unsteady regimes [6]. Hence, a completely quantitative explanation of our dynamics would require a thorough investigation of the hydrodynamics close to sliding unsteady contact lines.

To conclude, we have shown that sliding contact lines have a dramatic effect on the damping of liquid oscillations. It induces nonlinear dissipation, reminiscent of solid friction. We have proposed a successful predictive model, highlighting the crucial role of contact angle hysteresis. Perspectives include model refinement to account for the motion of the air-liquid interfaces, which can continue to

vibrate once the contact line is pinned. More importantly, we will revisit sloshing in tanks with this new quantitative view on contact line friction, to try to propose an operational prediction of its effect in the presence of the more complex, and possibly turbulent, sloshing flows.

We thank Emmanuel Kamwiziku for preliminary experiments, Lionel Bureau for experimental help, and Laurent Limat for fruitful discussions. This work was funded by CNRS (PICS 07952).

[1] O. M. Faltinsen and A. N. Timokha, *Sloshing* (Cambridge University Press, Cambridge, England, 2009).
[2] H. C. Mayer and R. Krechetnikov, Phys. Rev. E **85**, 046117 (2012).
[3] R. A. Ibrahim, *Liquid Sloshing Dynamics: Theory and Applications* (Cambridge University Press, Cambridge, England, 2005).
[4] G. H. Keulegan, J. Fluid Mech. **6**, 33 (1959).
[5] B. Cocciaro, S. Faetti, and M. Nobili, J. Fluid Mech. **231**, 325 (1991).
[6] L. Jiang, M. Perlin, and W. W. Schultz, Phys. Fluids **16**, 748 (2004).
[7] N. Le Grand, A. Daerr, and L. Limat, J. Fluid Mech. **541**, 293 (2005).
[8] N. Gao, F. Geyer, D. W. Pilat, S. Wooh, D. Vollmer, H. J. Butt, and R. Berger, Nat. Phys. **14**, 191 (2018).
[9] J. Ferrand, L. Favreau, S. Joubaud, and E. Freyssingeas, Phys. Rev. Lett. **117**, 248002 (2016).
[10] J. Delannoy, S. Lafon, Y. Koga, E. Reyssat, and D. Quéré, Soft Matter **15**, 2757 (2019).
[11] T. S. Ramakrishnan, P. Wu, H. Zhang, and D. T. Wasan, J. Fluid Mech. **872**, 5 (2019); J. C. Magniez, F. Zoueshtiagh, and M. Baudoin, J. Fluid Mech. **838**, 165 (2018).
[12] H. K. Moffatt, Nature (London) **404**, 833 (2000).
[13] F. Viola, P. T. Brun, B. Dollet, and F. Gallaire, Phys. Fluids **28**, 091701 (2016).
[14] See Supplemental Material at http://link.aps.org/supplemental/10.1103/PhysRevLett.124.104502 for more details on (i) a discussion on film deposition and on the force from dynamic menisci, (ii) an analytical resolution of our model, (iii) a refinement of our model in the case of nonuniform tube radius, and (iv) the relaxation of the air-water interface, which includes Refs. [15–17].
[15] E. J. Hinch, *Perturbation Methods* (Cambridge University Press, Cambridge, England, 1991).
[16] M. Iguchi, M. Ohmi, and K. Maegawa, Bull. JSME **25**, 1398 (1982).
[17] F. Moisy, M. Rabaud, and K. Salsac, Exp. Fluids **46**, 1021 (2009).
[18] J. Eggers, Phys. Rev. Lett. **93**, 094502 (2004).
[19] J. H. Snoeijer and B. Andreotti, Annu. Rev. Fluid Mech. **45**, 269 (2013).
[20] I. Cantat, Phys. Fluids **25**, 031303 (2013).
[21] A. Sauret, F. Boulogne, J. Cappello, E. Dressaire, and H. A. Stone, Phys. Fluids **27**, 022103 (2015).
[22] L. Landau and E. Lifshitz, *Mécanique des fluides*, 3rd ed. (Mir, Moscow, 1994).
[23] S. A. Berger, L. Talbot, and L. S. Yao, Annu. Rev. Fluid Mech. **15**, 461 (1983).
[24] J. C. Biery, AIChE J. **15**, 631 (1969).
[25] L. D. Landau and E. M. Lifshitz, *Mechanics*, 2nd ed. (Pergamon Press, Oxford, 1969).
[26] O. V. Voinov, Fluid Dyn. **11**, 714 (1976).
[27] R. G. Cox, J. Fluid Mech. **168**, 169 (1986).
[28] $A = \ln \ell_{\mathrm{macro}}/\ell_{\mathrm{micro}}$ with $\ell_{\mathrm{macro}} \approx 1$ mm a macroscopic length scale where the confining dimensions of the experiment, or large-scale physical effects such as gravity, begin to matter; and $\ell_{\mathrm{micro}} \approx 1$ nm a microscopic length scale where slip length of noncontinuum effects become significant [19]. The precise value of A, and the subsequent discussion in our paper, is quite insensitive on the precise values of ℓ_{macro} and ℓ_{micro}.
[29] K. G. Winkels, I. R. Peters, F. Evangelista, M. Riepen, A. Daerr, L. Limat, and J. H. Snoeijer, Eur. Phys. J. Spec. Top. **192**, 195 (2011).
[30] B. A. Puthenveettil, V. K. Senthilkumar, and E. J. Hopfinger, J. Fluid Mech. **726**, 26 (2013).
[31] P. G. Petrov and J. G. Petrov, Langmuir **8**, 1762 (1992).
[32] M. J. de Ruijter, J. De Coninck, and G. Oshanin, Langmuir **15**, 2209 (1999).
[33] L. Limat, J. Fluid Mech. **738**, 1 (2014).